

Creation of a Long-Acting Nanoformulated 2',3'-Dideoxy-3'-Thiacytidine

Dongwei Guo, MS,*† Tian Zhou, MS,*† Mariluz Araínga, PhD,† Diana Palandri, BS,† Nagsen Gautam, PhD,* Tatiana Bronich, PhD,* Yazen Alnouti, PhD,* JoEllyn McMillan, PhD,† Benson Edagwa, PhD,† and Howard E. Gendelman, MD*†

Background: Antiretroviral drug discovery and formulation design will facilitate viral clearance in infectious reservoirs. Although progress has been realized for selected hydrophobic integrase and nonnucleoside reverse transcriptase inhibitors, limited success has been seen to date with hydrophilic nucleosides. To overcome these limitations, hydrophobic long-acting drug nanoparticles were created for the commonly used nucleoside reverse transcriptase inhibitor, lamivudine (2',3'-dideoxy-3'-thiacytidine, 3TC).

Methods: A 2-step synthesis created a slow-release long-acting hydrophobic 3TC. Conjugation of 3TC to a fatty acid created a myristoylated prodrug which was encased into a folate-decorated poloxamer 407. Both in vitro antiretroviral efficacy in human monocyte-derived macrophages and pharmacokinetic profiles in mice were evaluated for the decorated nanoformulated drug.

Results: A stable drug formulation was produced by poloxamer encasement that improved monocyte-macrophage uptake, antiretroviral activities, and drug pharmacokinetic profiles over native drug formulations.

Conclusions: Sustained release of long-acting antiretroviral therapy is a new therapeutic frontier for HIV/AIDS. 3TC depot formation in monocyte-derived macrophages can be facilitated through stable subcellular internalization and slow drug release.

Key Words: lamivudine, nanoformulations, myristoylation, monocyte-macrophages, folic acid receptor, long-acting antiretroviral therapy

(*J Acquir Immune Defic Syndr* 2017;74:e75–e83)

INTRODUCTION

Long-acting nanomedicines introduced into antiretroviral therapeutic regimens have impacted the treatment of HIV infection.¹ Nanoformulated antiretroviral therapy (nanoART) can improve patient adherence, decrease toxicities, and sustain viral suppression.^{2–5} However, a challenge to bring nanoART to the forefront of antiretroviral therapy rests in how best to nanoformulate a broad range drugs that affect dosing intervals. This is highlighted by rapid drug clearance, low intracellular absorption, and suboptimal biodistribution. Toxicities that reduce clinical effectiveness support a need for improved drug delivery, optimization, and encapsulation for long-term treatment strategies and inevitable eradication.^{6–9}

Nucleoside reverse transcriptase inhibitors are the backbone of combination ART.^{10–12} Lamivudine (3TC) inhibits the transcription of HIV viral RNA to DNA by competing with cytidine for incorporation into viral DNA catalyzed by the viral reverse transcriptase enzyme, resulting in DNA chain termination after incorporation of the 3TC phosphorylated anabolite in place of endogenous cytidine triphosphate and plays an important role in ART regimens.¹³ 3TC has potent antiviral effects on HIV-1 and -2 and hepatitis-B virus.^{14–17} However, the drug is <36% protein bound and with a half-life of 5–7 hours and rapid renal elimination is cataloged as a short-acting drug.¹⁸

One means to extend the half-life of 3TC is by creating a hydrophobic prodrug. N-myristoyltransferase (NMT) affects myristoylation of proteins observed during the HIV life cycle.^{19–23} Fatty acid analogs of myristic acid can inhibit NMT and can be used to convert a hydrophilic 3TC into a hydrophobic drug.^{24–26} In particular, Agarwal et al were the first to demonstrate that myristoylated conjugates of nucleoside reverse transcriptase inhibitors that included 3TC could elicit significantly higher antiretroviral potency against the virus when compared to native drugs. Also, the scientific team showed that cellular uptake of the drug was improved markedly and secured intracellular hydrolysis after treatment.^{19,20} With this in mind, myristoylated 3TC (M3TC) was synthesized and then formulated into nanosuspensions. Folic acid (FA), which

Received for publication May 12, 2016; accepted August 8, 2016.

From the Departments of *Pharmaceutical Sciences; and †Pharmacology and Experimental Neuroscience, University of Nebraska Medical Center, Omaha, NE.

Supported by ViiV Healthcare and National Institutes of Health grants P01 DA028555, R01 NS36126, P01 NS31492, 2R01 NS034239, P01 MH64570, P01 NS43985, P30 MH062261, and R01 AG043540.

The authors have no conflicts of interest to disclose.

Supplemental digital content is available for this article. Direct URL citations appear in the printed text and are provided in the HTML and PDF versions of this article on the journal's Web site (www.jaids.com).

Correspondence to: Howard E. Gendelman, MD, Department of Pharmacology and Experimental Neuroscience, 985880 Nebraska Medical Center, Omaha, NE 68198-5930 (e-mail: hegendel@unmc.edu).

Copyright © 2016 The Author(s). Published by Wolters Kluwer Health, Inc. This is an open-access article distributed under the terms of the Creative Commons Attribution-Non Commercial-No Derivatives License 4.0 (CCBY-NC-ND), where it is permissible to download and share the work provided it is properly cited. The work cannot be changed in any way or used commercially without permission from the journal.

binds folate receptor expressed on activated macrophages, was attached to drug nanoparticles to facilitate cellular drug uptake and carriage.^{27,28} Such modifications facilitated drug retention in monocyte-macrophages.²⁹ M3TC nanoformulations with folate as a targeting ligand improved its antiretroviral efficacy and pharmacokinetic (PK) behavior. The formulation of a 3TC prodrug to create a novel long-term antiretroviral therapy has potential clinical impact.

METHODS

Reagents and Antibodies

3TC was a generous gift from GlaxoSmithKline Inc. (Research Triangle Park, NC). Poloxamer 407 (P407) and CF488-succinimidyl ester (CF488) were purchased from Sigma-Aldrich (St. Louis, MO). Sephadex LH-20 was from GE Healthcare (Piscataway, NJ). Pooled human serum was purchased from Innovative Biologics (Herndon, VA). Macrophage colony-stimulating factor was prepared from 5/9 m alpha3-18 cells (ATCC; CRL-10154) as previously described.³⁰ Rabbit anti-human antibodies to Rab5, Rab7, Rab11, and Rab14 and Alexa Fluor 568 goat anti-rabbit IgG were purchased from Santa Cruz Biotechnology (Dallas, TX).

Nanoformulated M3TC Manufacture and Characterization

A hydrophobically modified 3TC derivative (designated M3TC) was synthesized according to the scheme illustrated in Figure 1 and described in the Supplemental Digital Content,³¹ <http://links.lww.com/QAI/A900>. M3TC nanoparticles were formulated by high-pressure homogenization (Avestin EmulsiFlex-C3; Avestin Inc., Ottawa, ON, Canada), using P407 and folate-decorated P407 (FA-P407) to encase the drug crystals. The FA-P407 polymer was synthesized as previously described.²⁹ Nontargeted M3TC formulation (NM3TC) and targeted M3TC formulation (FA-NM3TC) were characterized as previously described.^{32,33}

Preparation of Dye-Labeled Nanoformulated M3TC

CF488 conjugated P407 was synthesized as previously described.²⁹ For preparation of CF488-labeled NM3TC, CF488-P407 and P407 were dissolved in methanol at a weight ratio of 1:4. The solvent was evaporated, and the mixture was resuspended with 10 mM HEPES to yield a 0.5% surfactant solution. M3TC was added at a 1% weight ratio and used to prepare CF488-labeled NM3TC nanoformulations.

NM3TC Particle Drug Release

To determine particle drug release, 100 μ mol NM3TC or FA-NM3TC particles were dispersed in 4 mL of phosphate-buffered saline (PBS) and placed into a 10-kDa dialysis tube in 2 L of PBS with stirring at 37°C. At 0.5, 1, 2, 4, 8, and 12 hours and 1, 2, 3, 5, 7, 9, and 12 days, 100 μ L of the suspension was collected from the dialysis tube and

dissolved in 900 μ L methanol.³⁴ M3TC in the aliquot was quantitated by high-performance liquid chromatography.

NM3TC Particle Cell Uptake

Human monocytes were obtained by leukapheresis from HIV-1 and -2 and hepatitis-B-seronegative donors and then purified by countercurrent centrifugal elutriation.³⁵ Human monocytes were plated in a 12-well plate at a density of 1.5×10^6 cells per well. After 7 days of differentiation, monocyte-derived macrophages (MDM) were treated with 100 μ M NM3TC. Uptake of NM3TC was assessed by measures of cell drug concentration without medium changes for 8 hours. Adherent MDM were scraped into PBS at 1, 2, 4, and 8 hours after treatment. Cells were pelleted by centrifugation at 1000g for 8 minutes at 4°C. Cell pellets were briefly sonicated in 200 μ L of methanol and centrifuged at 20,000g for 10 minutes at 4°C. Drug content was determined by reversed phase high-performance liquid chromatography with UV/Vis detection at 272 nm. Cell extracts were separated on a Phenomenex Synergi 4 μ m Hydro-RP column (150 \times 4.6 mm) using 20% 5.0 mM Na₂HPO₄/80% acetonitrile pumped at 1.0 mL/min. Drug content was quantitated by comparison of peak area to those of known standards (0.04–200 μ g/mL in methanol).

Antiretroviral Responses

Antiretroviral efficacy was determined by measurements of HIV reverse transcriptase (RT) activity. MDM were treated with 100 μ M 3TC, M3TC, or NM3TC for 4 hours. After treatment, cells were washed 3 times with PBS and cultivated with fresh medium. At 0, 5, 10, and 15 days after treatment, cells were challenged with HIV-1_{ADA} at a multiplicity of infection of 0.1 infectious particles per cell. After viral infection, the cells were cultured for another 7 days with half-medium exchanges every other day. Culture fluids were collected on day 7 for the measurement of RT activity as previously described.³⁶

Immunocytochemistry and Confocal Microscopy

For immunofluorescence staining, cells were washed 3 times with PBS and fixed with 4% paraformaldehyde at room temperature for 30 minutes. The cells were treated with blocking/permeabilizing solution (0.1% Triton, 5% BSA in PBS) and quenched with 50 mM NH₄Cl for 15 minutes. The cells were washed once with 0.1% Triton in PBS and sequentially incubated with primary and secondary antibodies at room temperature. Slides were covered in a ProLong Gold AntiFade reagent with DAPI (4',6-diamidino-2-phenylindole) and imaged using a \times 63 oil objective on an LSM 510 confocal microscope (Carl Zeiss Microimaging, Inc., Dublin, CA).³⁷ Zeiss LSM 510 Image browser AIM software version 4.2 was used to determine the number of pixels and the mean intensity of each channel.³²

HIV-1 p24 Staining

Cells in all treatment groups were fixed with 4% phosphate-buffered paraformaldehyde for 15 minutes at room

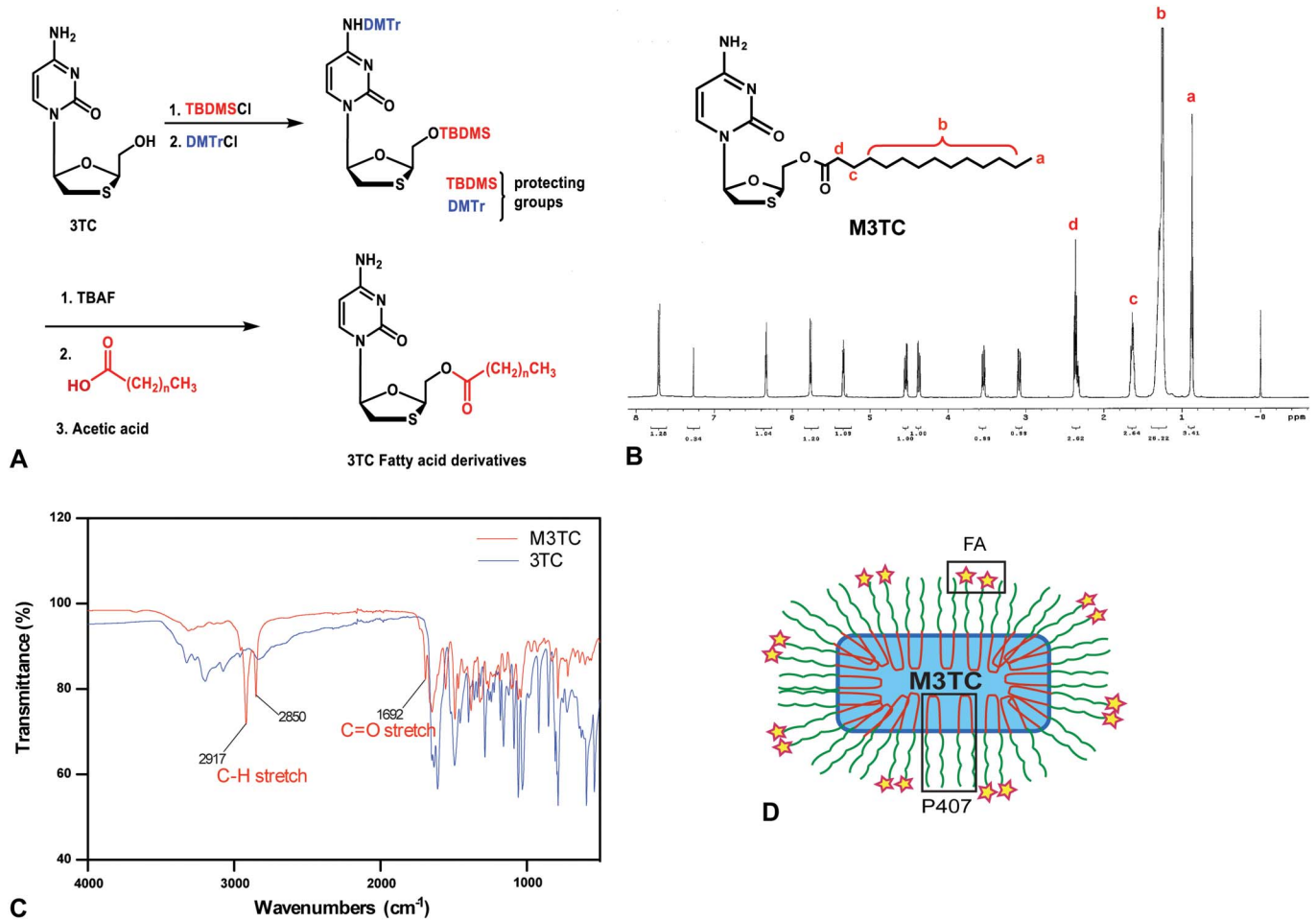


FIGURE 1. Scheme for the generation of myristoylated 3TC. A, Synthesis of myristoylated 3TC (M3TC) derivative. B, The proton nuclear magnetic resonance (¹H-NMR) spectrum of M3TC. Chemical shifts are reported in parts per million (ppm). C, Fourier transform infrared spectroscopy spectra of M3TC and native 3TC. D, Schematic diagram of the FA nanoformulated myristoylated 3TC (FA-NM3TC) formulation. FA-coated poloxamer 407 was used to encase hydrophobic M3TC into FA-NM3TC.

temperature. The fixed cells were blocked with 10% BSA in PBS containing 1% Triton X-100 for 30 minutes at room temperature and incubated with mouse monoclonal antibodies to HIV-1 p24 (1:100; Dako, Carpinteria, CA) for 3 hours at room temperature. Immunostaining was performed as described previously.^{32,38}

Pharmacokinetic Profiles

Male Balb/cJ mice (Jackson Labs, Bar Harbor, ME) were maintained on a folate-deficient diet (Harlan Teklad TD.00434; Harlan Laboratories, Inc., Indianapolis, IN) beginning 2 weeks before drug administration. Mice were injected with native 3TC, M3TC, NM3TC, or FA-NM3TC (equivalent to 50 mg 3TC/kg) intramuscularly (IM) in a volume of 50 μL/25 g mouse. For injections, 3TC was dissolved in PBS, M3TC was suspended in a mixture of ethanol-Cremophor EL-propylene glycol-PBS (43-5-20-32, vol/vol), NM3TC and FA-NM3TC were diluted with 10 mM HEPES to 47 mg M3TC/mL. Around 50 μL blood was collected by cheek bleeding at 8 hours, and 1, 3, 5, 7, 10, and 14 days after drug administration. Plasma and tissue preparation and ultra

performance liquid chromatography tandem mass spectrometry (UPLC-MS/MS) analysis are described in the Supplemental Digital Content, <http://links.lww.com/QAI/A900>.

Statistics

Data were analyzed by one-way analysis of variance and Tukey multiple-comparison test using GraphPad Prism (GraphPad Software, Inc., La Jolla, CA). The cell-based experiments were replicated 3 times and animal experiments were replicated 3 times. Animal treatment groups contained a minimum of 5 animals per group (n = 5). No outliers from animal or cell experiments were excluded. Differences were considered significant at a P-value of <0.05.

RESULTS

Characterization of Chemically Modified 3TC

M3TC was synthesized successfully as supported by the ¹H-NMR and Fourier transform infrared spectroscopy

spectra in Figure 1B, C. In the $^1\text{H-NMR}$ spectrum, chemical shifts of 0.9 and 1.3 ppm represented the 1° (RCH_3) and 2° (R_2CH_2) aliphatic protons derived from the fatty acid chain. The protons connected to the ester ($-\text{H}_2\text{C}-\text{COOR}$) contributed to the peak at 2.4 ppm. In the Fourier transform infrared spectroscopy spectrum, the wavenumbers of 2917 and 2850 cm^{-1} were attributed to the C–H stretch, which belonged to the alkyl derivative derived from the fatty acid chain conjugated to the native 3TC; the wavenumber of 1692 cm^{-1} was attributed to the C=O stretch from the ester bond. The solubility of the hydrophobic M3TC was determined to be $100\text{ }\mu\text{g/mL}$ in water, compared to 70 mg/mL for 3TC.

Characterization of NM3TC

The nanoformulations were manufactured by high-pressure homogenization. Particle size, charge, and polydispersity index (PDI) for all formulations were determined by dynamic light scattering. A schematic of the targeted M3TC particles is illustrated in Figure 1D, and the physicochemical characteristics of different formulations are summarized in Figure 2A. For FA-NM3TC, a 40% FA-P407/60% P407 polymer solution was used to formulate the M3TC. As seen in Figure 2A, the hydrodynamic diameter of FA-NM3TC was $433 \pm 23\text{ nm}$ (PDI = 0.25) and is only slightly larger than that of NM3TC ($375 \pm 21\text{ nm}$, PDI = 0.21). The zeta potential of FA-NM3TC was similar to that of NM3TC. High drug loading (75.0% for NM3TC and 76.9% for FA-NM3TC) and encapsulation efficiency (96.3% for NM3TC, 98.4% for FA-NM3TC) were observed for both formulations.

NM3TC Particle Drug Release

The release of drug from NM3TC and FA-NM3TC nanoformulations is illustrated in Figure 2B. There was no significant burst release during the first 2 hours. After 8 hours, M3TC release reached 67.1% and 27.3% for NM3TC and FA-NM3TC, respectively. Sustained M3TC release was seen over 5 days. The cumulative M3TC release reached 70.0% on day 3 and 94.8% on day 12 for NM3TC, and 76.4% on day 3 and 96.7% on day 12 for FA-NM3TC.

Macrophage Uptake

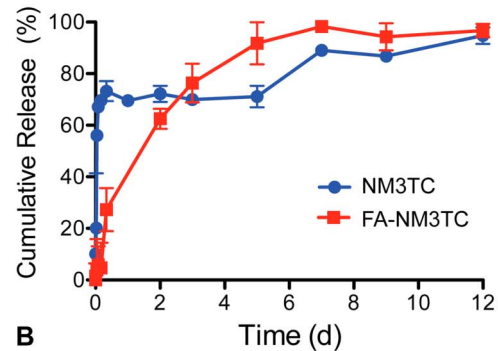
As shown in Figure 2C, the uptake of both NM3TC and FA-NM3TC increased over time to reach a maximum at 2 hours. At 2 hours, the cell drug concentration was $24.9\text{ }\mu\text{g}/10^6$ cells for FA-NM3TC, which was more than 2-fold greater than that of NM3TC ($10.4\text{ }\mu\text{g}/10^6$ cells). After 2 hours, cell drug levels began to decrease, and drug levels for NM3TC and FA-NM3TC at 8 hours were 2.1 and $2.8\text{ }\mu\text{g}/10^6$ cells, respectively.

Antiretroviral Activities of Nanoformulated M3TC

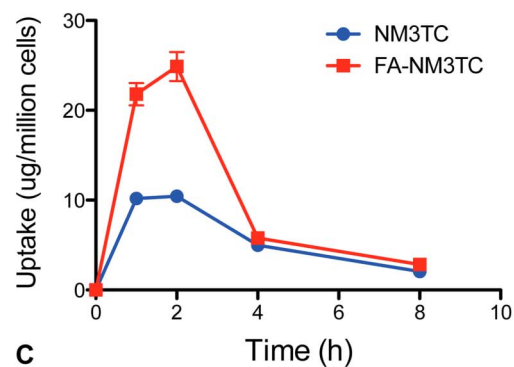
To assess the antiretroviral activity of NM3TC and FA-NM3TC, HIV RT activity was determined in HIV-1-

Formulation	NM3TC	FA-NM3TC
Size	$375 \pm 21\text{ nm}$	$433 \pm 23\text{ nm}$
PdI	0.21 ± 0.03	0.25 ± 0.03
Zeta-potential	$-21.0 \pm 0.8\text{ mV}$	$-19.7 \pm 1.3\text{ mV}$
Drug loading	75.0%	76.9%
Encapsulation efficiency	96.3%	98.4%
FA-P407	0	40%

A



B



C

FIGURE 2. Characterization of M3TC nanoformulations. A, Physicochemical characteristics of M3TC nanoformulations. B, Cumulative release of M3TC in isotonic solution. C, Time course of uptake of M3TC nanoformulations in human MDM. MDM were treated with $100\text{ }\mu\text{M}$ nanoformulations (based on M3TC content) for 1, 2, 4, and 8 hours. The cell lysates at indicated times were analyzed by high-performance liquid chromatography for M3TC quantification. Data represent the mean \pm standard error of the mean ($n = 3$), for each time point.

infected culture medium from MDM pretreated with 3TC, NM3TC or FA-NM3TC at 0, 5, 10, or 15 days before infection. Significant differences were observed between cells treated with native 3TC or either M3TC nanoformulation. For native 3TC treated cells, RT activity was suppressed only in the day 0 group. In contrast, for nanoformulation-treated groups, sustained antiretroviral activities were observed. The RT activities were suppressed to $<25\%$ during the first 10 days. At day 15, the RT activities for NM3TC and FA-NM3TC were 59.8% and 68.5%, respectively, compared with 110.0% for the native 3TC group. Significant differences

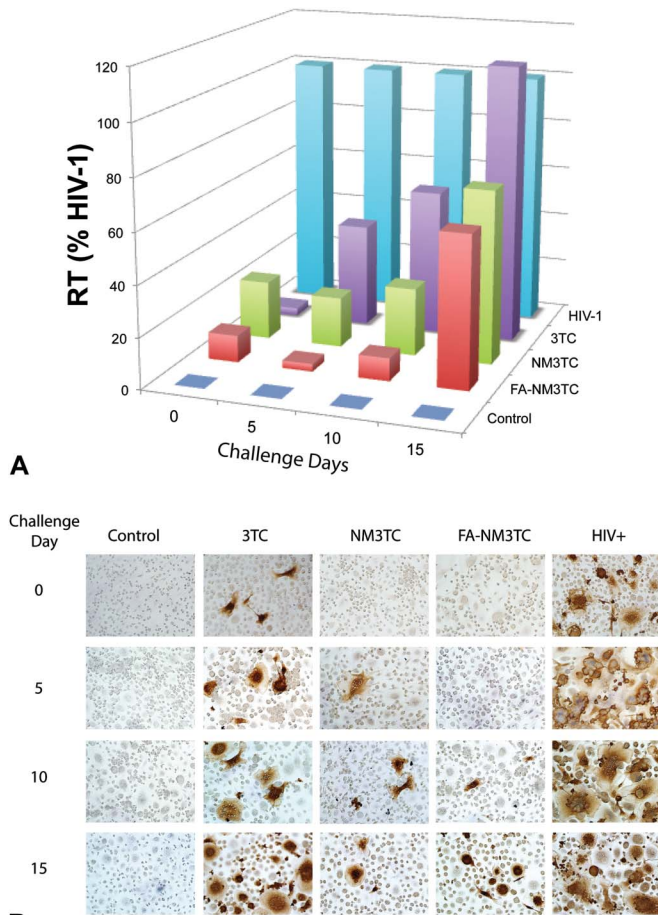


FIGURE 3. Antiretroviral activities of 3TC and M3TC and nanoformulated M3TC (NM3TC and FA-NM3TC). **A**, HIV-1 RT activity of native 3TC and nanoformulated M3TC. **B**, HIV-1 p24 staining of virus-infected MDM pretreated with native 3TC or nanoformulated M3TC. MDM were treated with 100 μM native 3TC, NM3TC, or FA-NM3TC for 4 hours. At days 0, 5, 10, or 15, MDM were infected with HIV-1 for 4 hours. Uninfected cells without treatment served as a negative control; HIV-1-infected cells without treatment served as a positive control for the RT assay. All the samples were collected after 7 days of viral infection for RT assay and HIV-1 p24 staining. For RT activity, results are shown as the mean of 5 replicates. The differences between 3TC and NM3TC or FA-NM3TC at days 5, 10, and 15 are significant ($P < 0.05$). The differences between NM3TC and FA-NM3TC are significant at days 0, 5, and 10 ($P < 0.05$).

were observed between NM3TC and FA-NM3TC during the first 10 days ($P < 0.05$), and FA-NM3TC showed greater antiretroviral activity compared with NM3TC; however, the difference was not significant at day 15 (Fig. 3A). These results were confirmed by HIV-1 p24 staining (Fig. 3B). NM3TC and FA-NM3TC showed greater antiretroviral activity compared with native 3TC, and much less p24 staining was observed in these 2 groups. FA-NM3TC showed greater suppression of viral replication especially in the first 10 days, when little to no HIV-1 p24 antigen was detected in MDM treated with FA-NM3TC.

Immunocytochemistry and Confocal Microscopy

To assess subcellular behavior of the nanoformulated M3TC, fluorescently labeled nanoparticles were used to visualize colocalization of endolysosomal proteins and NM3TC. CF488-labeled NM3TC was prepared and Rab5, 7, 11, and 14 were selected as target endolysosomal proteins. NM3TC distributed in a punctate pattern throughout the cytoplasm and perinuclear cell regions (Figure 4). NM3TC was found predominantly in late (Rab7) and recycling (Rab11 and 14) endosomes, and this immunofluorescence colocalization demonstrated that NM3TC was taken into and stored in macrophages through the endolysosomal pathways. Our previous studies have demonstrated that the HIV reservoir exists mainly in late and recycling endosomes, and HIV-1 and nanoformulations deregulated cellular proteins in an opposing manner,³³ supporting the idea of subcellular-targeted nanoparticles for long-acting antiretroviral therapy.

Pharmacokinetic Profiles

Balb/cJ mice were administered 3TC, M3TC, NM3TC, FA-NM3TC (equivalent to 50 mg 3TC/kg in PBS) to determine their PK profiles according to the scheme shown in Figure 5A. Plasma 3TC concentrations after treatment were analyzed by UPLC-MS/MS and data are presented in Figure 5B, C. At all time points, M3TC plasma concentrations were lower than the detection limit. M3TC is unstable in plasma and converts to 3TC completely within a few minutes after spiking. Higher and more sustained 3TC levels were observed in both nanoformulation-treated groups compared to native or prodrug treatment and plasma drug levels were maintained over 10 days for both nanoformulations. At day 1, no 3TC could be detected in plasma from the native 3TC-treated group; whereas 3TC plasma levels in the M3TC, NM3TC, and FA-NM3TC groups were 58.7 ± 6.9 , 349.2 ± 12.5 , and 383.2 ± 13.8 ng/mL, respectively. At day 3, less than 0.7 ng/mL 3TC was detected in plasma from the M3TC-treated group, whereas plasma drug levels for NM3TC and FA-NM3TC groups were 131.3 ± 18.1 and 151.6 ± 23.2 ng/mL, respectively. Compared with NM3TC, FA-NM3TC showed prolonged drug release and plasma drug levels were more than 2-fold higher than those of NM3TC from day 5 to day 14. At day 14, the plasma 3TC level for FA-NM3TC was 22.7 ± 12.5 ng/mL, whereas that for NM3TC was at or below the limit of quantitation (<0.7 ng/mL). Tissue 3TC levels at 14 days are shown in Figure 5D. Drug levels in liver, spleen and lymph nodes were approximately 2-fold higher after FA-NM3TC treatment than NM3TC treatment (25–40 ng/g versus 5–15 ng/g, respectively). No drug was detected in tissues from 3TC- or M3TC-treated animals.

DISCUSSION

In this study, we describe the synthesis of a long-acting hydrophobic 3TC prodrug and its subsequent nanoformulation. This was designed to improve its clinical bioavailability. Myristic acid was used to synthesize a hydrophobic drug. The 14-carbon alkyl chain significantly decreased the water solubility of native 3TC and improved the drug-protein and

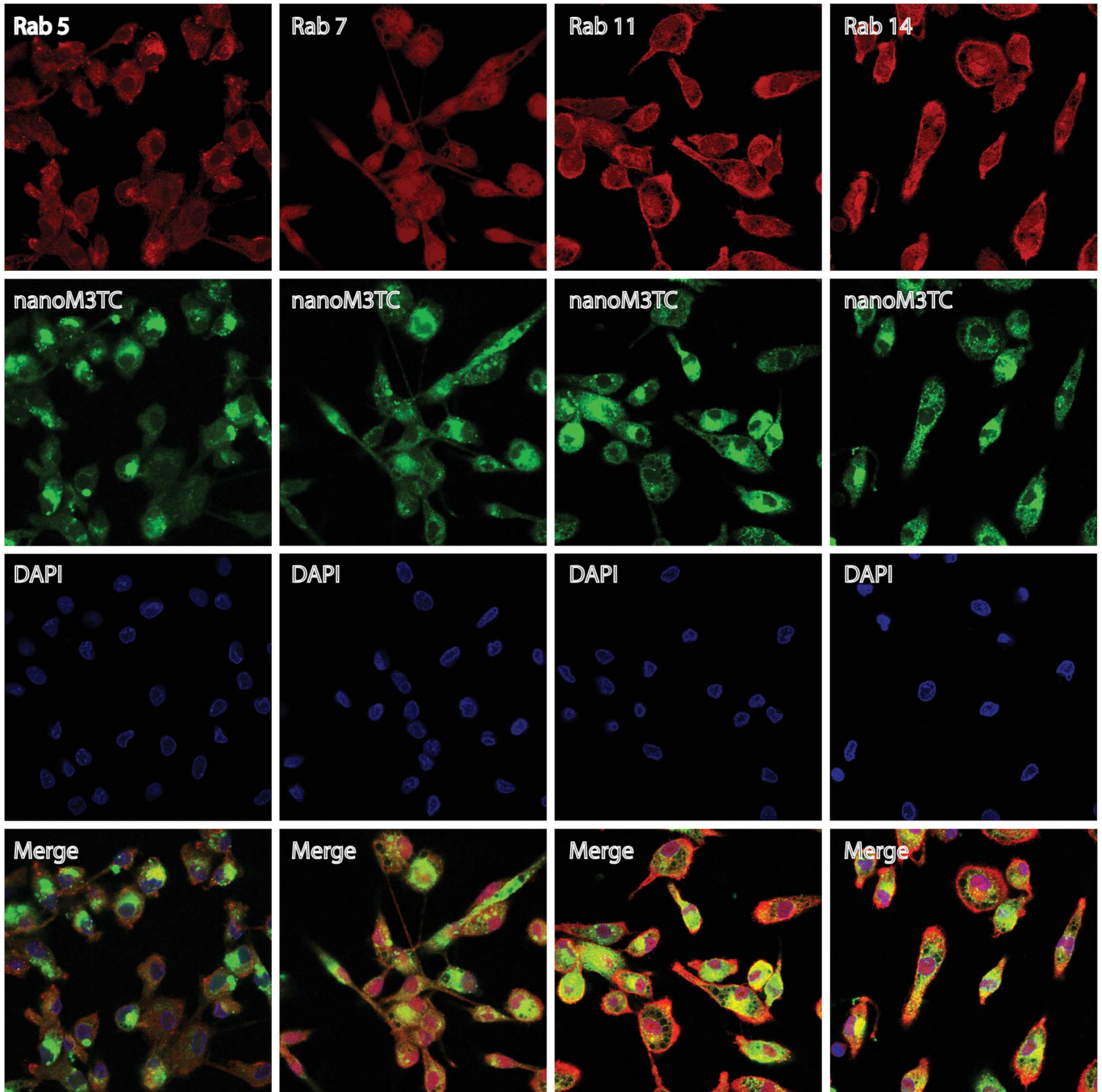


FIGURE 4. Subcellular localization of NM3TC in MDM. MDM were cultured for 7 days and treated with 100 μ M CF488-labeled NM3TC (nanoM3TC) for 4 hours. The cells were stained with Rab5, 7, 11, or 14 primary antibodies and Alexa Fluor 568-labeled secondary antibodies to visualize the corresponding cell compartments using confocal microscopy. Nanoparticles are shown in green, cell compartments in red, and nuclei in blue.

drug–membrane interactions when in the systemic circulation. The modified myristoylated 3TC was produced as a single compound and made through an orthogonal protecting group strategy. This was performed to ensure that only the hydroxyl functional group was derivatized. The ester bond used for fatty acid conjugation did not affect the antiretroviral efficacy of the prodrug because the ester bond could be

hydrolyzed in the presence of intracellular esterases, including lysosomal acid lipase, phospholipase, acetylhydrolase, nucleases, and lipoprotein lipase, which are localized mainly in lysosomes. Although speculative, the enzymes are well known to catalyze the breakdown of acyl groups and hydrolyze compounds taken into lysosomes. In our study, the hydrophobic M3TC presumably diffused through the cell

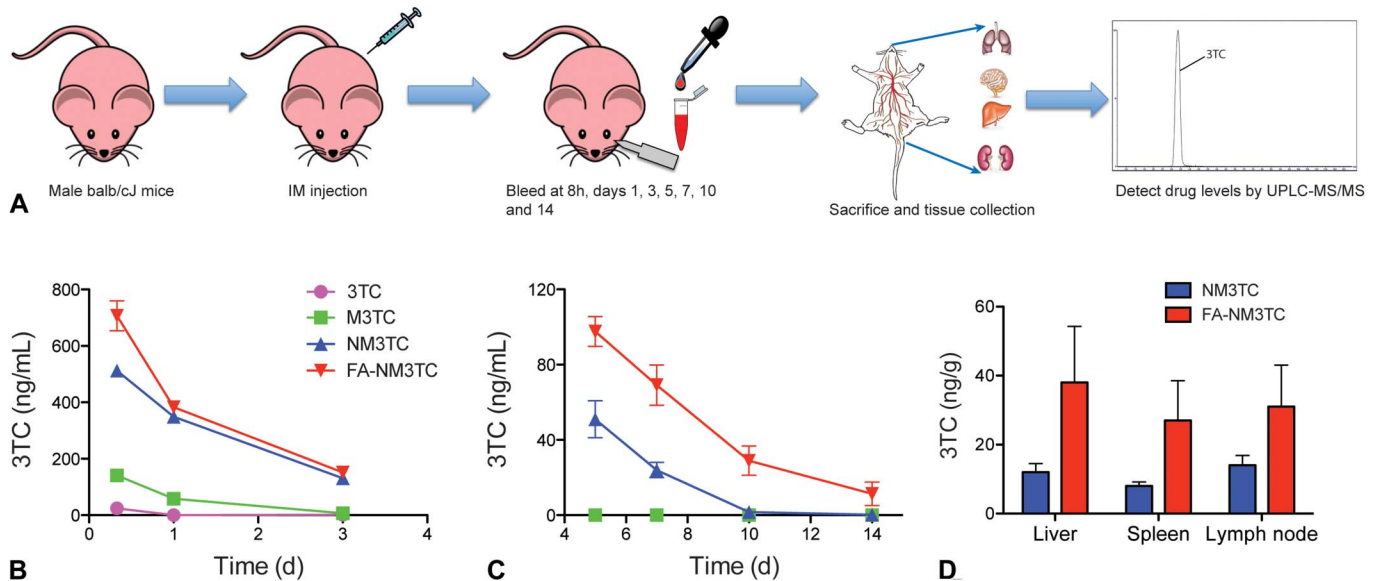


FIGURE 5. Plasma and tissue drug levels in Balb/cJ mice. A, Scheme of the in vivo study design. Mice were administered intramuscularly 50 mg/kg equivalents of 3TC using native 3TC, M3TC, NM3TC, or FA-NM3TC. Plasma was collected into acetonitrile for drug analysis at 8 hours, and days 1, 3, 5, 7, 10, and 14 after treatment; tissues were collected at day 14. B, Plasma drug levels from 8 hours to day 3. C, Plasma drug levels from day 5 to day 14. D, Drug levels in liver, spleen, and lymph nodes on day 14 after NM3TC or FA-NM3TC treatment. 3TC levels were determined by UPLC-MS/MS. Data are expressed as mean ± SEM (n = 5).

membrane into different cell compartments. The prodrug was transported into lysosomes, degraded by the esterases, and released the native 3TC to provide antiretroviral activity. Myristic acid formed during the conversion of prodrug into its active form can also contribute to the observed antiretroviral effect. Indeed, it has been reported that NMT is a crucial enzyme involved in catalyzing the myristoylation of capsid proteins p17, Pr160^{gag-pol}, and Pr55^{gag}, which are involved in the life cycle of HIV-1.²¹ Myristic acid has been shown to inhibit NMT.^{39–41} HIV-1 replication could, consequently, be inhibited by the myristoylated 3TC. Interestingly, M3TC particles exhibited antiretroviral efficacy comparable to that of native 3TC as demonstrated by the day 0 RT results, which indicates that the myristoylation did not alter the antiretroviral efficacy of native 3TC. Neither M3TC nor 3TC were cytotoxic at the concentration used as evaluated both by trypan blue exclusion and 3-(4,5-dimethylthiazol-2-yl)-2,5-diphenyltetrazolium bromide tests (data not shown). At high concentrations, myristoylated 3TC demonstrated reduced cytotoxicity compared with native 3TC which could be attributed to the enhanced drug hydrophobicity. Although intracellular 3TC–triphosphate formation was not measured, the potent antiretroviral responses support such events had taken place.

Nanocrystals are useful as drug delivery carriers because of their high drug-loading capacity, improved stability, and bioavailability.^{42,43} Nanocrystals can be coated with surfactant for enhanced cellular uptake and sustained cellular maintenance for long-acting efficacy. For drugs with a short half-life, such as 3TC, the therapeutic efficacy is limited and therefore nanocrystals are ideal platforms for increasing drug retention and improving systemic circulation.

P407 was used as a coating surfactant to prepare stable nanosuspensions and realize long-term drug release. Both FA-targeted and nontargeted M3TC nanoparticles were prepared with particle sizes of 350–430 nm and favorable PDI.

The FA-NM3TC nanoparticles exhibited better uptake by macrophages, especially during the first 2 hours. These particles would be expected to be taken up through both phagocytosis and receptor-mediated endocytosis. Folate derivatives are internalized mainly through the reduced folate carrier and the folate receptor (FR), which has a high affinity for FA.⁴⁴ There are several isoforms of FR including FR- α and FR- β , which are glycosylphosphatidylinositol-anchored protein receptors. We have demonstrated in previous studies that FA-coated nanoparticles are taken up by macrophages mainly through FR- β because of its overexpression in activated macrophages.²⁹ For HIV-1-infected patients, FR- β is expected to be highly expressed on macrophages because immune cells are activated in infected individuals.^{45,46} Meanwhile, nanoparticles can directly activate macrophages and stimulate FR- β overexpression on the cell membrane of macrophages.²⁹ Both folate-targeted and nontargeted M3TC formulations can be taken up by macrophages through clathrin-mediated endocytosis. Particles undergo recognition in the blood stream through opsonization; the opsonized particles attach to the cell membrane and are ingested into phagosomes.⁴⁷ FA-NM3TC can be internalized by macrophages preferentially through a clathrin-independent pathway through FR- β interaction. This process can facilitate the internalization of the M3TC particles, which can explain the 2-fold difference in cell drug levels after 2 hours of treatment for FA-NM3TC and NM3TC and the enhanced antiretroviral activity of FA-NM3TC compared to NM3TC. Owing to the

enhanced cell uptake, FA-NM3TC exhibited greater antiretroviral activity than nontargeted NM3TC as confirmed by HIV-1 RT activity and p24 staining. Greater protection against HIV-1 was observed for the targeted nanoformulation and significant differences remained for 10 days. Equivalent antiretroviral efficacy for both formulations by day 15 could be because most of the drug had been released by then; however, both nanoformulations showed greater antiretroviral efficacy compared to native 3TC.

Our previous work has demonstrated that endolysosomes can be dysregulated by HIV-1 infection through Rab protein expression; endosomes are also sites of active viral assembly, where virions accumulate during productive infection.^{32,33} Endolysosomal pathways are vital to the transport of antimicrobial drugs since they enable the drug particles to relocate at specific sites where virus replicates and is assembled. We investigated the intracellular localization of nontargeted M3TC particles in macrophages. We observed that they predominantly colocalized in late (Rab7) and recycling (Rab11 and 14) endosomes, which demonstrated that NM3TC was taken up and stored in macrophages through the endosomal pathways. M3TC particles contained within endocytic compartments would provide a protected environment to facilitate drug release with sustained antiretroviral efficacy. This not only provides effective drug delivery to HIV action sites for improved therapeutic efficacy but also protects the particles from intracellular degradation.

To determine the PK profiles of NM3TC, we treated the mice with 3TC, M3TC, NM3TC, and FA-NM3TC (equivalent to 50 mg 3TC/kg). Administration of NM3TC and FA-NM3TC led to a marked increase in 3TC plasma concentrations up to 10 days post injection compared to native 3TC. Importantly, the folate-coated M3TC nanoformulation exhibited 2-fold enhanced plasma and tissue 3TC levels compared with the noncoated formulation. After 2 weeks, the plasma 3TC levels for FA-NM3TC were still greater than 3 times higher than the half maximal effective concentration (EC₅₀) of 3TC of ~6.9 ng/mL. These studies also demonstrated that the targeted M3TC particles were more effectively stored in the macrophage depots after injection, as evidenced by their localization in reticuloendothelial tissues and lymph nodes. M3TC nanoparticles can be taken up by monocytes in blood and redistributed during systemic circulation to reticuloendothelial tissues. In macrophages, M3TC can then be gradually released into the endosomal compartments and converted to native 3TC by hydrolases. In vivo M3TC was efficiently converted to 3TC since little M3TC was detected in plasma and tissues. Through binding to the FR on macrophages, more FA-NM3TC particles could be taken up by monocyte/macrophages, distributed into different cellular compartments, and avoid degradation by lysosomes, all of which would explain the higher in vitro uptake and more sustained in vivo plasma and tissue drug levels for FA-NM3TC particles.

In conclusion a hydrophobic 3TC prodrug was successfully synthesized through myristoylation and incorporated into targeted and nontargeted nanocrystalline formulations to improve drug half-life and reduce cytotoxicity. NM3TC

exhibited enhanced macrophage uptake and sustained antiretroviral efficacy. FA-NM3TC exhibited improved PK. This novel drug delivery system has shown great potential for clinical application.

ACKNOWLEDGMENTS

The authors thank Ms. Janice Taylor of the UNMC Confocal Laser Scanning Microscopy Core.

REFERENCES

- Ross EL, Weinstein MC, Schackman BR, et al. The clinical role and cost-effectiveness of long-acting antiretroviral therapy. *Clin Infect Dis*. 2015;60:1102–1110.
- Cihlar T, Fordyce M. Current status and prospects of HIV treatment. *Curr Opin Virol*. 2016;18:50–56.
- Margolis DA, Brinson CC, Smith GH, et al. Cabotegravir plus rilpivirine, once a day, after induction with cabotegravir plus nucleoside reverse transcriptase inhibitors in antiretroviral-naïve adults with HIV-1 infection (LATTE): a randomised, phase 2b, dose-ranging trial. *Lancet Infect Dis*. 2015;15:1145–1155.
- Jackson A, McGowan I. Long-acting rilpivirine for HIV prevention. *Curr Opin HIV AIDS*. 2015;10:253–257.
- Gunawardana M, Remedios-Chan M, Miller CS, et al. Pharmacokinetics of long-acting tenofovir alafenamide (GS-7340) subdermal implant for HIV prophylaxis. *Antimicrob Agents Chemother*. 2015;59:3913–3919.
- Spivak AM, Planelles V. HIV-1 eradication: early trials (and tribulations). *Trends Mol Med*. 2016;22:10–27.
- Jourjy J, Dahl K, Huesgen E. Antiretroviral treatment efficacy and safety in older HIV-infected adults. *Pharmacotherapy*. 2015;35:1140–1151.
- Zhan P, Pannecouque C, De Clercq E, et al. Innovations and future Trends. *J Med Chem*. 2016;59:2849–2878.
- Nozza S, Svicher V, Saracino A, et al. State of the art of dual therapy in 2015. *AIDS Rev*. 2015;17:127–134.
- Russo G, Paganotti GM, Soeria-Atmadja S, et al. Pharmacogenetics of non-nucleoside reverse transcriptase inhibitors (NNRTIs) in resource-limited settings: influence on antiretroviral therapy response and concomitant anti-tubercular, antimalarial and contraceptive treatments. *Infect Genet Evol*. 2016;37:192–207.
- Clark DN, Hu J. Hepatitis B virus reverse transcriptase—target of current antiviral therapy and future drug development. *Antiviral Res*. 2015;123:132–137.
- Famigliani V, Silvestri R. Focus on chirality of HIV-1 non-nucleoside reverse transcriptase inhibitors. *Molecules*. 2016;21:221.
- Hill A, Sawyer W. Effects of nucleoside reverse transcriptase inhibitor backbone on the efficacy of first-line boosted highly active antiretroviral therapy based on protease inhibitors: meta-regression analysis of 12 clinical trials in 5168 patients. *HIV Med*. 2009;10:527–535.
- Lytvyak E, Montano-Loza AJ, Mason AL. Combination antiretroviral studies for patients with primary biliary cirrhosis. *World J Gastroenterol*. 2016;22:349–360.
- Li X, Jie Y, You X, et al. Optimized combination therapies with adefovir dipivoxil (ADV) and lamivudine, telbivudine, or entecavir may be effective for chronic hepatitis B patients with a suboptimal response to ADV monotherapy. *Int J Clin Exp Med*. 2015;8:21062–21070.
- Palacios R, Perez-Hernandez IA, Martinez MA, et al. Efficacy and safety of switching to abacavir/lamivudine (ABC/3TC) plus rilpivirine (RPV) in virologically suppressed HIV-infected patients on HAART. *Eur J Clin Microbiol Infect Dis*. 2016;35:815–819.
- Greig SL, Deeks ED. Abacavir/dolutegravir/lamivudine single-tablet regimen: a review of its use in HIV-1 infection. *Drugs*. 2015;75:503–514.
- Huang F, Allen L, Huang DB, et al. Evaluation of steady-state pharmacokinetic interactions between ritonavir-boosted BILR 355, a non-nucleoside reverse transcriptase inhibitor, and lamivudine/zidovudine in healthy subjects. *J Clin Pharm Ther*. 2012;37:81–88.
- Agarwal HK, Chhikara BS, Bhavaraju S, et al. Emtricitabine prodrugs with improved anti-HIV activity and cellular uptake. *Mol Pharm*. 2013;10:467–476.

20. Agarwal HK, Chhikara BS, Hanley MJ, et al. Synthesis and biological evaluation of fatty acyl ester derivatives of (-)-2',3'-dideoxy-3'-thiacytidine. *J Med Chem*. 2012;55:4861–4871.
21. Farazi TA, Waksman G, Gordon JI. The biology and enzymology of protein N-myristoylation. *J Biol Chem*. 2001;276:39501–39504.
22. Wu Z, Alexandratos J, Ericksen B, et al. Total chemical synthesis of N-myristoylated HIV-1 matrix protein p17: structural and mechanistic implications of p17 myristoylation. *Proc Natl Acad Sci U S A*. 2004;101:11587–11592.
23. Singh D, McMillan J, Hilaire J, et al. Development and characterization of a long-acting nanoformulated abacavir prodrug. *Nanomedicine (Lond)*. 2016;11:1913–1927.
24. Langner CA, Lodge JK, Travis SJ, et al. 4-oxatetradecanoic acid is fungicidal for *Cryptococcus neoformans* and inhibits replication of human immunodeficiency virus I. *J Biol Chem*. 1992;267:17159–17169.
25. Takamune N, Hamada H, Misumi S, et al. Novel strategy for anti-HIV-1 action: selective cytotoxic effect of N-myristoyltransferase inhibitor on HIV-1-infected cells. *FEBS Lett*. 2002;527:138–142.
26. Ohta H, Takamune N, Kishimoto N, et al. N-Myristoyltransferase 1 enhances human immunodeficiency virus replication through regulation of viral RNA expression level. *Biochem Biophys Res Commun*. 2015;463:988–993.
27. Paulos CM, Turk MJ, Breur GJ, et al. Folate receptor-mediated targeting of therapeutic and imaging agents to activated macrophages in rheumatoid arthritis. *Adv Drug Deliv Rev*. 2004;56:1205–1217.
28. Xia W, Hilgenbrink AR, Matteson EL, et al. A functional folate receptor is induced during macrophage activation and can be used to target drugs to activated macrophages. *Blood*. 2009;113:438–446.
29. Puligujja P, McMillan J, Kendrick L, et al. Macrophage folate receptor-targeted antiretroviral therapy facilitates drug entry, retention, antiretroviral activities and biodistribution for reduction of human immunodeficiency virus infections. *Nanomedicine*. 2013;9:1263–1273.
30. Clark SC. Interleukin-6. Multiple activities in regulation of the hematopoietic and immune systems. *Ann New York Acad Sci*. 1989;557:438–443.
31. Notari S, Sergi M, Montesano C, et al. Simultaneous determination of lamivudine, lopinavir, ritonavir, and zidovudine concentration in plasma of HIV-infected patients by HPLC-MS/MS. *IUBMB Life*. 2012;64:443–449.
32. Guo D, Zhang G, Wysocki TA, et al. Endosomal trafficking of nanoformulated antiretroviral therapy facilitates drug particle carriage and HIV clearance. *J Virol*. 2014;88:9504–9513.
33. Arainga M, Guo D, Wiederin J, et al. Opposing regulation of endolysosomal pathways by long-acting nanoformulated antiretroviral therapy and HIV-1 in human macrophages. *Retrovirology*. 2015;12:5.
34. Guo D, Li T, McMillan J, et al. Small magnetite antiretroviral therapeutic nanoparticle probes for MRI of drug biodistribution. *Nanomedicine (Lond)*. 2014;9:1341–1352.
35. Gendelman HE, Orenstein JM, Martin MA, et al. Efficient isolation and propagation of human immunodeficiency virus on recombinant colony-stimulating factor 1-treated monocytes. *J Exp Med*. 1988;167:1428–1441.
36. Kalter DC, Gendelman HE, Meltzer MS. Inhibition of human immunodeficiency virus infection in monocytes by monoclonal antibodies against leukocyte adhesion molecules. *Immunol Lett*. 1991;30:219–227.
37. Dou H, Destache CJ, Morehead JR, et al. Development of a macrophage-based nanoparticle platform for antiretroviral drug delivery. *Blood*. 2006;108:2827–2835.
38. Zhang G, Guo D, Dash PK, et al. The mixed lineage kinase-3 inhibitor URM-099 improves therapeutic outcomes for long-acting antiretroviral therapy. *Nanomedicine*. 2016;12:109–122.
39. Rampoldi F, Bonrouhi M, Boehm ME, et al. Immunosuppression and aberrant T cell development in the absence of N-Myristoylation. *J Immunol*. 2015;195:4228–4243.
40. Perinpanayagam MA, Beauchamp E, Martin DD, et al. Regulation of co- and post-translational myristoylation of proteins during apoptosis: interplay of N-myristoyltransferases and caspases. *FASEB J*. 2013;27:811–821.
41. Morgan CR, Miglionico BV, Engen JR. Effects of HIV-1 Nef on human N-myristoyltransferase 1. *Biochemistry*. 2011;50:3394–3403.
42. Nowacek AS, Balkundi S, McMillan J, et al. Analyses of nanoformulated antiretroviral drug charge, size, shape and content for uptake, drug release and antiviral activities in human monocyte-derived macrophages. *J Control Release*. 2011;150:204–211.
43. Kumar L, Verma S, Prasad DN, et al. Nanotechnology: a magic bullet for HIV AIDS treatment. *Artif Cells Nanomed Biotechnol*. 2015;43:71–86.
44. Zaki NM, Tirelli N. Gateways for the intracellular access of nanocarriers: a review of receptor-mediated endocytosis mechanisms and of strategies in receptor targeting. *Expert Opin Drug Deliv*. 2010;7:895–913.
45. Hattori Y, Sakaguchi M, Maitani Y. Folate-linked lipid-based nanoparticles deliver a NFκB decoy into activated murine macrophage-like RAW264.7 cells. *Biol Pharm Bull*. 2006;29:1516–1520.
46. Kularatne SA, Low PS. Targeting of nanoparticles: folate receptor. *Methods Mol Biol*. 2010;624:249–265.
47. Sahay G, Alakhova DY, Kabanov AV. Endocytosis of nanomedicines. *J Control Release*. 2010;145:182–195.